TU Delft

Delft University of Technology

Infrared absorbance of vertically-aligned multi-walled CNT forest as a function of synthesis temperature and time

Gheitaghy, Amir Mirza; Ghaderi, Amir; Vollebregt, Sten; Ahmadi, Majid; Wolffenbuttel, Reinoud; Zhang, Guo Qi

DOI
10.1016/j.materresbull.2020.110821

Publication date
2020

Document Version
Accepted author manuscript

Published in
Materials Research Bulletin

Citation (APA)
Gheitaghy, A. M., Ghaderi, A., Vollebregt, S., Ahmadi, M., Wolffenbuttel, R., & Zhang, G. Q. (2020). Infrared absorbance of vertically-aligned multi-walled CNT forest as a function of synthesis temperature and time. *Materials Research Bulletin*, *126*, Article 110821. https://doi.org/10.1016/j.materresbull.2020.110821

Important note
To cite this publication, please use the final published version (if applicable).
Please check the document version above.

Copyright
Other than for strictly personal use, it is not permitted to download, forward or distribute the text or part of it, without the consent of the author(s) and/or copyright holder(s), unless the work is under an open content license such as Creative Commons.

Takedown policy
Please contact us and provide details if you believe this document breaches copyrights.
We will remove access to the work immediately and investigate your claim.

This work is downloaded from Delft University of Technology.
For technical reasons the number of authors shown on this cover page is limited to a maximum of 10.

Infrared absorbance of vertically-aligned multi-walled CNT forest as a function of synthesis temperature and time

Amir Mirza Gheytaghi[1*], Amir Ghaderi[2], Sten Vollebregt[1], Majid Ahmadi[3], Reinoud Wolffenbuttel[2,4], and Guo Qi Zhang[1]

[1] Laboratory of Electronic Components, Technology and Materials, Department of Microelectronics, Delft University of Technology, 2628 CD, Delft, The Netherlands

[2] Electronics Materials and systems, Department of Microtechnology and Nanoscience, Chalmers University of Technology, 412 96, Gothenburg, Sweden

[3] Kavli Institute of Nanoscience, Department of Applied Science, Delft University of Technology, 2628 CD, Delft, The Netherlands

[4] Electronic Instrumentation Laboratory, Department of Microelectronics, Delft University of Technology, 2628 CD, Delft, The Netherlands

Abstract

In this paper, the growth of optimized vertically aligned multi-walled carbon nanotube (VA-MWCNT) forests by LPCVD method for use in a large-area absorber in infrared detectors is presented. The effect of synthesis temperature (500−700 °C) and time (1−10 min) on the optical absorption coefficient in the infrared (2−20 μm) is investigated by FT-IR measurement at various incident angles (15-80°). The structural properties of VA-MWCNT are characterized by SEM, TEM and Raman spectroscopy. Spectral measurements show an increasing absorption with the height of the forest that results at increased synthesis time and temperature. However, the absorption coefficient decreases with increasing synthesize time and temperature, while it is also affected by other properties, such as diameter, density, alignment, and uniformity. Moreover, the reduction in absorption at oblique incident angles demonstrates the relevance of surface properties. Finally, a circular graphite waveguide system is used to model the absorption characteristics of an MWCNT forest.

Keywords: VA-MWCNT; mid-infrared; forest; growth time; growth temperature.

*Corresponding author. E-mail: a.mirzagheytaghi@tudelft.nl (Amir Mirza Gheytaghi), Tel. +31616517023

1. Introduction

The tunability of the optical, electrical and mechanical properties of Carbon Nanotubes (CNTs) has made it a widely researched material. Several interesting optical properties have been observed in vertically aligned (VA) CNT arrays, such as photonic crystal effects [1, 2], directional emission [3, 4], wavelength-selective emission and polarization-dependent reflection [5, 6], and high absorptivity [7, 8] which can potentially be utilized in many optical applications. VACNTs exhibit high absorbance of light over a spectrum ranging from the visible to infrared wavelength region, due to inter-band transitions and free-electron absorption, while it provides impedance matching to air [9]. As a result, CNT thin films and coatings are a promising material for applications that involve thermal radiation detection or heat transfer. Applications include solar thermal energy generation [10], blackbodies [11], thermal control [12], baffles and shrouds [13], field emitter array [14],and radiometers for electromagnetic power measurement in wavelengths from THz to optical (ultra-violet) [15]. Within this context, an improved understanding of the optical and radiative properties of CNT films in the broad infrared wavelength region is essential for enabling an optimization.

The unique optical property of VACNT forest of being an almost perfect blackbody absorber depends both on the atomic structure of each individual CNT and on their collective arrangement. The optical properties of a single-walled (SW) CNT exhibits a strong dependence on the detailed atomic structure [16, 17]. Due to the difficulty of chirality-controlled growth or chirality separation of SWCNT, engineering of optical properties and functionalities is complicated. In contrast, multi-walled (MW) CNTs, due to their larger size, have more regular and uniform optical properties. As a result, it has become common practice to treat each MWCNT as a homogeneous medium [17], structured to meet the requirements of a particular application.

The favourable blackbody absorption and emission properties of VA-MWCNTs are mainly because of the low volume ratio of CNTs to air, which results in a low refractive index and in turn to enhances the impedance matching to air [18, 19]. The density [20] and height [21] of VACNT are likely additional reasons for the efficient and wideband absorption of the incident light. CNTs reveal several interesting characteristics when used as a blackbody material, such as the colourful iridescence reflected from the substrate if the height of VACNTs is less than 500 nm [22]. The reflectance can be limited to 15% using micromechanical treatment of the top surface of vertically aligned CNTs, which makes it suitable for different applications [23, 24]. The polarized reflectance from tip bent VACNTs at broadband wavelength has also been studied [5]. Furthermore, vertically aligned CNT arrays have received attention for their potential for introducing anisotropic reflectance properties [25]. Finally, also the specular reflectance from arrays of VACNTs at different wavelengths over a certain incident angle has been studied [26].

Several methods are available for the synthesis of MWCNT's, such as arc discharge, laser ablation and different types of chemical vapour depositions (CVD) [27]. Low-pressure (LP) CVD is preferred for large- area synthesis, because of the spatial uniformity of thickness and purity, simple handling, high reliability, homogeneity of deposited layers and high reproducibility that results from the well-controlled process and its cleanroom compatibility. The LPCVD technique improves the purity by removing unwanted gaseous molecules on the surface of MWCNT during the growth process [28]. The optical properties of an MWCNT array further depend on how the MWCNTs are arranged, including pattern, alignment, height, and inter-tube distance. It is of great interest to identify the effect of factors such as the nanotubes diameter, number of walls, and degree of graphitization during the synthesis process on the optical properties of MWCNT. Therefore, the parameters optimization is an important factor during synthesis. Santangelo et al. optimized the CVD growth of CNT-based hybrids using the Taguchi method [29]. Among the parameters, the synthesis temperature and time are the crucial factors in controlling MWCNT formation as well as its degree of graphitization.

Here, the experimental study of the influence of growth temperature and growth time on absorption efficiency of VA-MWCNTs is reported with the objective of finding the settings for maximum absorbance. The morphology of the forest is characterized by height, density, diameter and uniformity (as can be revealed by SEM). Also, investigating the quality can be quantified by using the Raman spectroscopy and can be seen the presence of defects by TEM. Total absorbance measurements were taken in the 2-20 μm spectral range and correlated to the forest's specific morphology. The results of this study show a relationship between the height and the quality of the MWCNT forest and the resulting optical property. The objective of this work is to enhance the understanding of LPCVD MWCNT production for a more-predictable result and improved optical characteristics, which may pave the way for the acceptance of the MWCNT forest as a material for optical devices and enable applications ranging from solar thermal absorbers, solar photovoltaic cells to electronic devices.

2. Experimental Methods

2.1. Fabrication process

VA-MWCNT were grown by LPCVD in a commercial deposition system (Black Magic Pro, Aixtron) on a (100) p-type silicon substrate. The synthesis method has the advantages of well-controlled growth at the silicon wafer level in a cleanroom compatible process with patterning possibility. Orientation, growth rate, length, diameter, and density of CNTs can be controlled by changing the synthesis temperature and time according to a previously tuned recipe [30]. As shown in

Figure **1**, the first step involves the growth of a 500 nm thick thermal silicon oxide layer on a silicon wafer, to electrically insulate the support layer from the substrate. Next, a 10/50 nm thin layer of

titanium/titanium nitride (Ti/TiN) is reactively sputtered on the substrate to prevent diffusion of the iron (Fe) and allow the formation of Fe nanoparticles in order to nucleate CNT. Subsequently, a 5 nm thin layer of Fe catalyst is deposited by electron beam evaporation. Next, VA-MWCNTs are grown using a gas flow mixture of 700 sccm hydrogen over 50 sccm acetylene (H_2/C_2H_2) at 80 mbar. Finally, the substrate is cooled down in a N_2 atmosphere. Various growth temperatures in the range of 500-700 ºC with 50 ºC intervals and 10 minutes growth time are used to investigate the effect of quality, as determined by Raman spectroscopy, of the CNT structure on the optical absorption. In order to investigate the effect of the CNT forest height, the growth time is also changed from 1 to 10 min at a constant temperature set at 650 ºC.

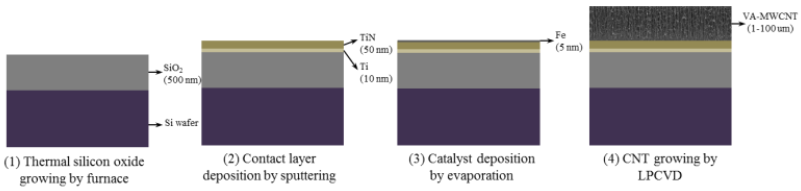

Figure 1. Schematic flowchart of the fabrication process of VA-MWCNT

2.2. Sample characterization

The morphology and microstructure of VACNT forest patterns were determined by an FEI XL50 scanning electron microscope (SEM). The nanostructure of one MWCNT was observed by Transmission Electron Microscopy (TEM) using an FEI Titan microscope operating at an acceleration voltage of 300 keV with tungsten filament. For preparing the samples to TEM, the following steps are taken: dissolving the MWCNT forest into an ethyl alcohol, dispersing with ultrasonic for 10 min and pouring one drop of solution onto a copper grid covered by an amorphous carbon film.

The Raman spectra were measured directly on the CNT forest using a Renishaw inVia system with a He-Ne laser as excitation source at 633nm. Raman spectroscopy is one of the most powerful tools for fast and non-destructive analysis of CNTs without sample preparation. Raman yields information about the purity, defects and tube alignment, while it also provides signature information to distinguish MWCNTs from other carbon allotropes [31]. We gathered three measurements from each sample under identical conditions and fitted the average of the resulting band data from the three separate measurements.

Fourier transform infrared spectroscopy (FTIR, Bruker, VERTEX) was used to characterize the absorption spectrum of the deposited MWCNTs in the mid-infrared to the far infrared range (2-20 μm). Measuring the reflectance of the samples, while assuming zero transmission through the sample, the absorption of the MWCNTs can be calculated (A=1-R). The reflectance was measured using a reflectance module installed in an FTIR sample compartment. The aperture was selected as 1 mm, and both the incident and measurement angle were varied from 15° to 80°. According to the specifications, an aperture of 1 mm corresponds to a spot size smaller than 3.6 mm in diameter up to 80° incident angle.

3. Results and discussion

3.1. Structure characteristics

The morphology of VACNTs is very important for their radiative interaction. The height variation of VACNTs synthesized under different temperatures (between 500-700 ºC with 50 ºC intervals) within 10 min growth is captured in the SEM images presented in Figure 2. It is evident that the morphology and the length of the CNTs strongly depend on the growth temperature. For lower growth temperatures (less than 550 ºC), the short CNTs grow as mats with comparatively low density. Though well-aligned, high-density vertical growth of the MWCNTs was obtained for a temperature range of 600–700 ºC, the height was found to be at maximum for the nanotubes grown at 650 ºC. It is possible that at this temperature, the precursor was sufficiently pyrolyzed and the good interaction between the hydrocarbon and catalyst facilitated the formation of uniform nanotube diameter and good alignment within the bundle. Generally, the solubility and mobility of Fe increase with temperature, which could cause particle coalescence. Moreover, the H_2 etching reaction speed also increases with temperature. As this process is diffusion dominated, carbon diffuses into the Fe catalyst and at a particular temperature, iron has a limited solubility [32]. The growth rate depends on the growth temperature and varies from less than 1 μm/min at 500 ºC low temperatures to several μm/min at higher temperatures.

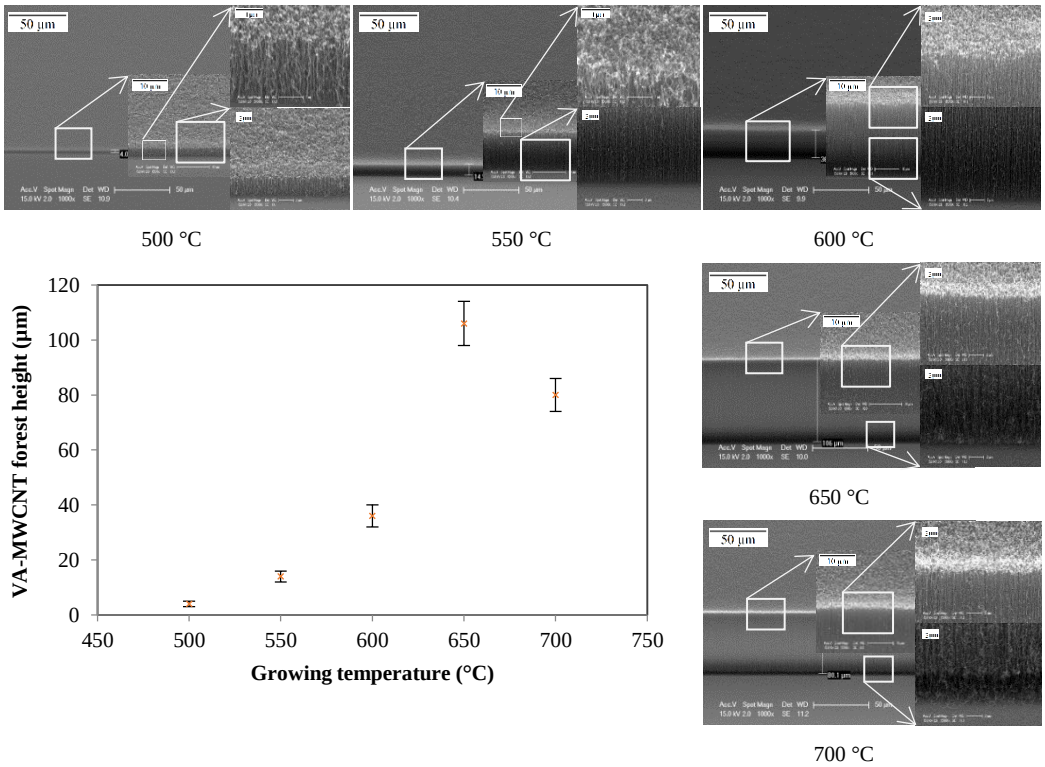

Figure 2. VA-MWCNT forest height versus growth temperature for 10 min growth time

Figure 3 shows the SEM images and dependence of CNT forest height on growth duration at 650 ºC. The plot shows that the height increases almost linearly with time at an average growth rate of 10.7 µm/min. Beyond a certain timescale, the growth rate decreases and length saturate at a constant value. Ubnoske et al. [33] proposed a growth kinetics model based on Fick's law in order to understand the effect of time and temperature on CNT growth which confirms the current results.

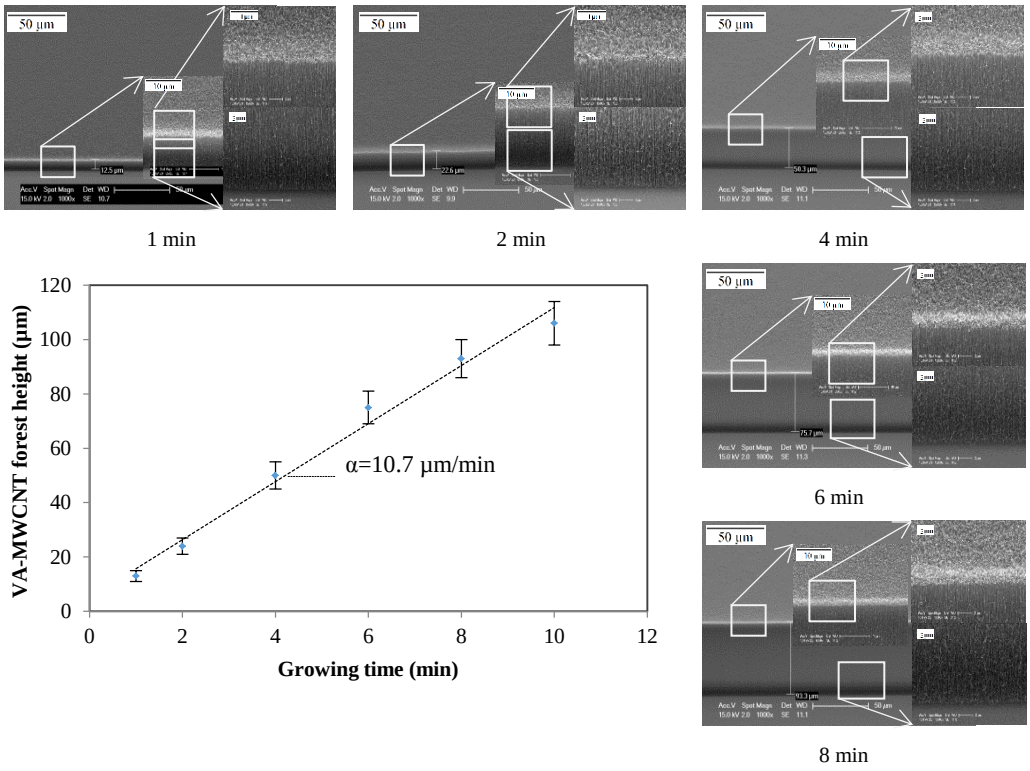

Figure 3. VA-MWCNT forest height versus growth time at 650 °C growth temperature

Raman analysis was used to investigate the effect of the growth parameters on the quality of the CNT forest. Normalized Raman data with respect to the G-band of MWCNTs at various synthesized temperatures and times, as shown in Figure 4, consist of main bands centred around 1580 cm^{-1} (G-band), 2660 cm^{-1} (2D- or G′-band), 1330 cm^{-1} (D-band), and 1610 cm^{-1} (D′-band) and several low-intensity bands. The G-band corresponds to the tangential stretching mode of sp^2 carbon and suggests the CNTs to be composed of crystalline graphitic carbon. The D-band and D′-band originate from any kind of disorder in the sp^2 -hybridized carbon and indicates lattice distortions in the curved graphene sheets, tube ends, defects, etc. On the other hand, the G′-band attributed to the overtone of the D-band, which becomes stronger when less graphitic sheets and/or defects are present. The strongest weak band at 2930 cm^{-1} is the combined overtone of the D- and G-band, called D+G. Finally, the band around 3233 cm^{-1} is

explained as being an overtone of the D′-band (2D′). The absence of any bands under 300 cm^{-1} shows the absence of SWCNTs [34].

The Raman spectra are fitted using the non-linear least squares curve fitting routines of Matlab to determine the location, magnitude, and width of the different bands. The approach for plotting the resulting ratios and widths of the bands versus growth temperature and time is available in the literature [35]. Typical approaches to use Raman spectroscopy for assessment of quality rely on the intensity ratio of the D-band and the G-band. Unfortunately, the interpretation of D/G data is not straightforward, due to the effect of carbon impurities on these intensities [36]. DiLeo et al. [37] published a report where the ratio of the G′-band with respect to the D-band is shown to provide a more accurate alternative for measuring MWCNT quality and purity. The reason originates from the fact that the G′-band results from a two-phonon process, which causes its intensity to be particularly sensitive to the sample purity, as the disorder would not allow for the coupling effect necessary for the two-phonon process.

As the CNT growth temperature is increased, the G′/G ratio increases, indicating better ordering and structuring within the tubes [35]. The G′-band is nearly equal to G-band at growing temperature of 700 °C indicates the high quantity of structural defects and is usually correlated to MWNTs, due to a greater number of defects, originated from multiple graphite layers. For CNT growth at 600 °C, the D/G ratio is 2.5 with a distinctive sharp D-band. The D-band originates from a hybridized vibrational mode associated with graphene edges and indicates the presence of some defects in the graphene layers, most likely due to the bamboo or cup-shaped structure inside each CNT, as illustrated by the TEM image in Figure 5. The D peak decreases some-what as a function of increasing growth temperature, consistent with annealing nanocrystalline graphite to form slightly larger nanodomains . A decrease in the D/G ratio and increase in G′/G ratio in higher temperature than 600 °C, is indicative of the decrease of impurities and enhancement of quality.

Changing the synthesizing time has less effect on Raman parameters than changing the temperature. D/G initially decreases and subsequently increases by growth time. The variations of parameters are less than ~10% and therefore, the quality of the deposited film remains almost unchanged over the thickness of the film. At a short growth time less than 4 min, the CNT could be less aligned, thus causing more defects. At longer growth time more than 4 min, growth speed can be reduced for the same length, thus giving the H_2 more opportunity to keep the tips of the CNT clean from a-C.

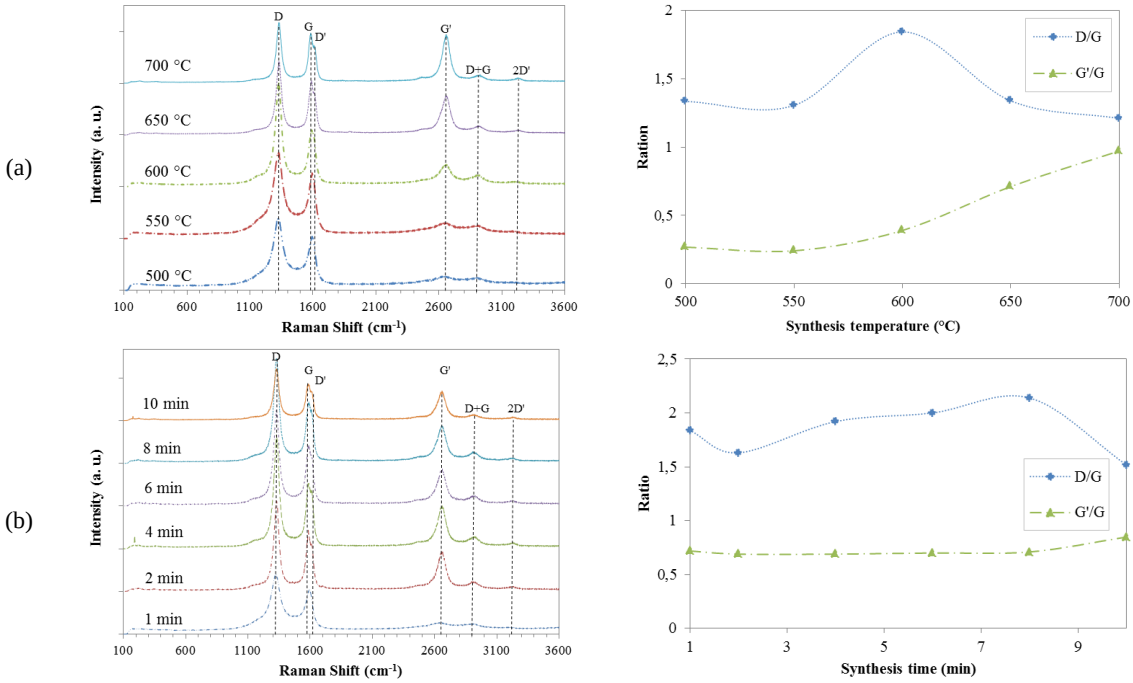

Figure 4. Raman result of CNT growth (a) at different temperatures for 10 min; (b) for different times at 650 °C.

The TEM analysis of the CNT synthesized at different temperatures and times, as shown in Figure 5, reveal more details than SEM and Raman analysis. It was observed that all CNTs exhibit multi-walled tubular structures, with evenly spaced lattice fringes in an almost equal number of fringes on either side of the central hollow core. The average interlayer spacing for all CNTs, as taken over 15-20 graphene shells, was found to be in the range of 0.33 nm to 0.35 nm. The constituent graphene layer is essentially crystalline but contains various structural defects at low-temperature growth [38]. For example, there are some broken graphene layers, forming some steps and kinks along both the inner and outer walls of CNTs. There are also some bamboo crossings graphene layers formed in the inner side of CNT walls, which probably result because the stress in the wall cannot be released at low temperature. Meanwhile, some amorphous carbon was found on the outer wall of CNTs. These structural defects destroy the perfection of graphene shells and make both the inner and outer walls defective and rougher compared to high-temperature grown CNTs, whose walls are commonly made of clean, straight, ordered, and highly crystalline graphene layers.

For CNT arrays that were grown at 550 °C, the mean diameter is 21±2 nm, which increases to 30±3 nm when the growth temperature was elevated to 650 °C. The CNT diameter versus time is also shows nearly linear growth behaviour, compatible with Kaatz et al. thermodynamics model [39]. The diameter distribution of the as-grown CNTs strongly depends on the size distribution of the catalyst particles [40]. A higher growth temperature increases the collision frequency in gas phase, so that catalyst particles in

larger size formed. The sintering possibility also increases, so that the small particles are prone to agglomerate into larger ones by Ostwald ripening. As a result, the as-formed iron catalyst particles become larger in size and CNTs with a larger diameter in array form are synthesized. At higher temperature (700 °C), as-produced graphitic shell around the catalyst particles prevent further reaction for growth (often referred to as catalyst poisoning) and thus reduces catalyst lifetime and limits array height and diameter [41]. Table 1 summarizes the structural characteristics of the synthesized VA-MWCNT in terms of diameter, length, and Raman ratio parameters.

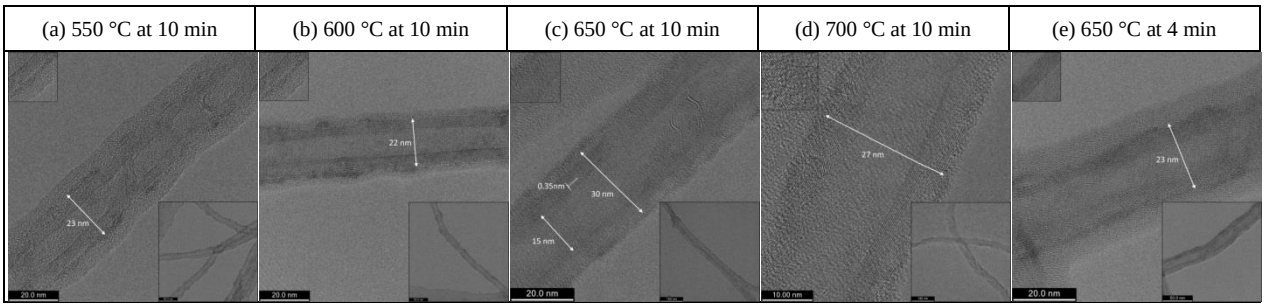

Figure 5. TEM images of single MWCNT growth at different temperatures for 10 min and at 650 ℃ for 4 min.

Table 1. Summary of diameter and length and Raman parameters of synthesized VA-MVCNT samples

Growing condition	Diameter (nm)	Length (μm)	D/G	G′/G
500 ℃ – 10 min	18±4	4±1.4	1.33	0.26
550 ℃ – 10 min	21±4	14±2.3	1.30	0.24
600 ℃ – 10 min	22±5	36±4.1	1.84	0.39
650 ℃ – 10 min	30±7	106±8.6	1.34	0.71
700 ℃ – 10 min	27±6	80±6.2	1.21	0.97
650 ℃ – 1 min	17±2	13±2.8	1.84	0.72
650 ℃ – 2 min	19±4	24±3.3	1.63	0.69
650 ℃ – 4 min	23±3	50±5.1	1.92	0.69
650 ℃ – 6 min	27±4	75±7.3	2.00	0.70
650 ℃ – 8 min	29±6	93±8.7	2.14	0.71

3.2. Optical characteristics

The incident light entering a CNT forest is reflected and absorbed multiple times by the individual nanotubes, before it makes its way out of the forest. The surface reflection from vertically aligned CNT forests is considerably lower than non-aligned CNTs, resulting in a higher absorbance of the light [42]. Furthermore, the absorption (and emissivity) of the CNT increases with the area mass density (i.e. height x density) [43], suggesting thick CNT layers for applications where high absorption is required. However, for many applications, especially in MEMS, a thin layer is often required. In a thermal detector for instance, the thermal mass of the absorber decreases the sensitivity and time response of the detector. Optimizing the CNT composition to ensure high absorption at low thicknesses is essential for satisfying the requirements in MEMS applications.

The absolute reflectance of the VA-MWCNT samples were measured using an FTIR spectrometer (Bruker, VERTEX) equipped with a variable angle specular reflectance module (Bruker, A513/Q) over the near to far-infrared (2-20 μm). The minimum incidence angle possible with the reflectance module was 15^{o} and was used to measure the reflectance at a near-normal incidence angle. The transmittance of the double side polished substrate with the catalyst layer was also measured to be below 0.001.

Figure 6 shows the schematic of the light propagation in an MWCNT layer with a thickness *t*. The measured reflectance is a function of the reflectance at the interface between air and CNT (R_{CNT}), CNT and substrate (R_{sub}), and the absorption coefficient of the CNT. In a typical CNT forest, the R_{CNT} is primarily due to the misaligned CNT layers [44]. Here for a vertically aligned CNT layers, we assume the R_{CNT} to be negligible. Since R_{sub} is expected to be high, the main contribution to the measured reflectance is due to the light passing through the CNT twice. Therefore, the measured reflectance can be written as

$$R \approx e^{-2\alpha t} \quad (1)$$

where α is the absorption coefficient and *t* is the thickness of the CNT layer.

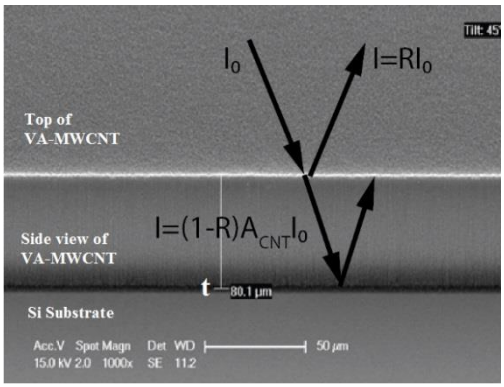

Figure 6. Schematics of light absorption and propagation in an MWCNT layer.

Figure 7 (a) shows the measured reflectance spectra of MWCNT samples grown at 650 °C. The noisy raw reflection data is low pass filtered using a Gaussian filter with a window size of 190 cm^{-1} to result in smooth absorption curve. SEM images in Figure 3 showed a nearly constant and uniform forest density over the length of the CNT. Furthermore, as the surface morphology of the CNTs constant similar with the different thicknesses, its effect on the absorption is neglected in this analysis. The reflection is well below 10% for all samples and increases slightly over the measurement range. The absorbance is calculated using A = 1 – R and shown in Figure 7 (b).

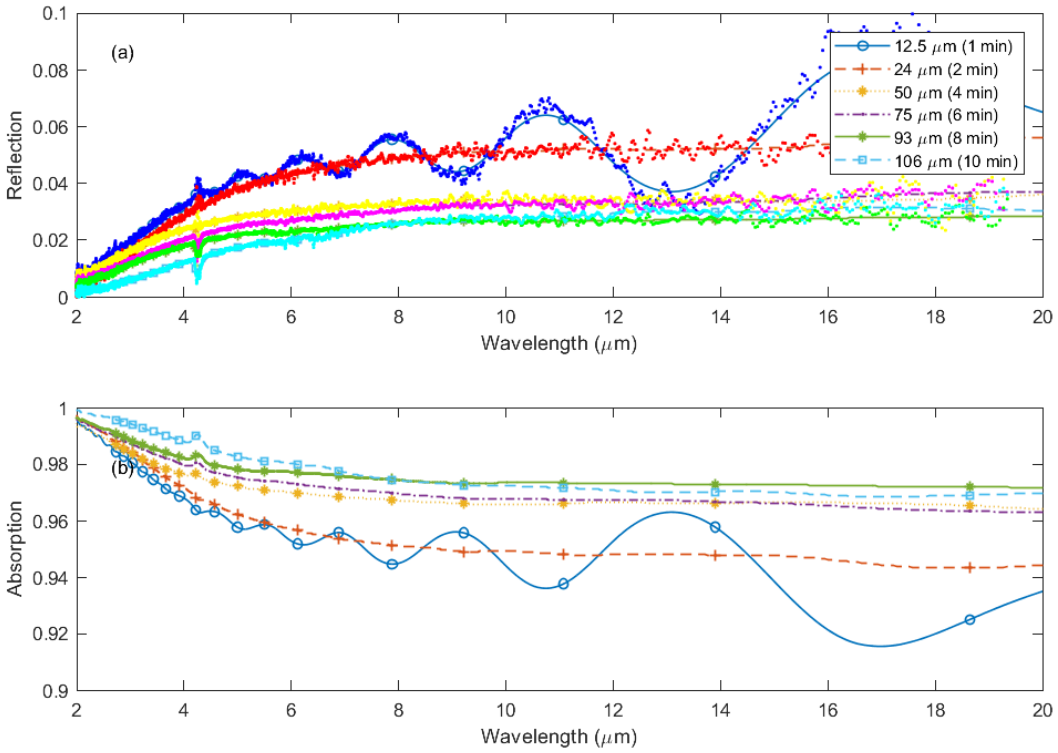

Figure 7. (a) Reflection and (b) absorption at an incident angle of 15° for MWCNT forests growth at different times. The scatter plot in (a) shows the unfiltered reflection data.

The absorption coefficient was calculated from the absorption using $\alpha = -1/(2t.\ln R)$ and is shown in Figure 8. The absorption coefficient decreases with increasing wavelength at short wavelengths and remains almost constant over the range between 5 and 20 μm. Moreover, the calculated absorption coefficient of the CNT decreases with the layer thickness as defined by forest length, which is consistent with the literature [44]. Therefore, comparing CNTs with different composition must be performed at the same thickness range.

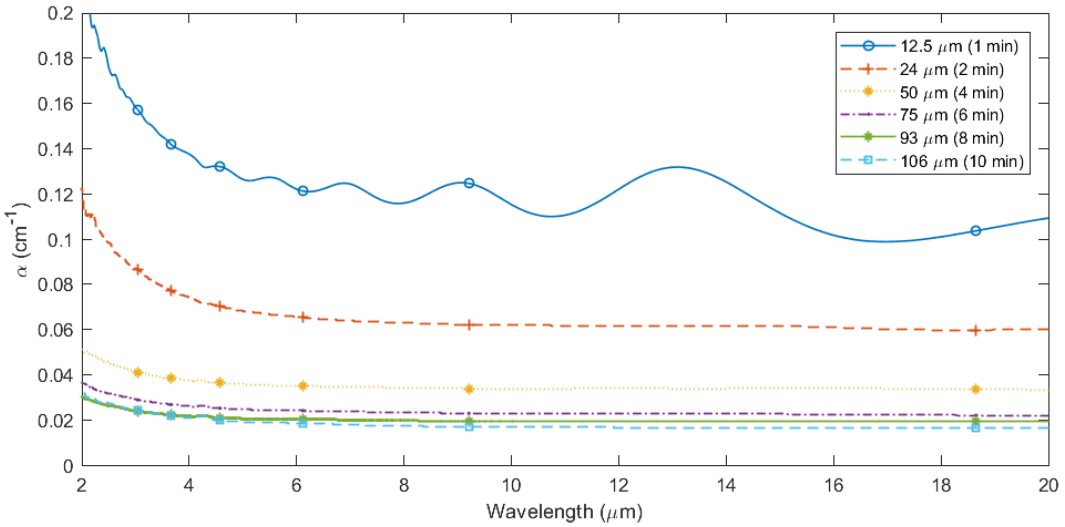

Figure 8. Absorption coefficient at an incident angle of 15° for MWCNT forests of different thickness grown at 650 °C.

The growth temperature of VA-MWCNT changes the morphology of the CNT and consequently the absorption. To validate this effect the growth temperature was varied from 550 to 700 ^{o}C and the absorption coefficient was measured. The deposition time was kept constant at 10 min. As shown in Figure 2, the height and density of the CNT increases with temperature.

Figure 9 shows the absorption and absorption coefficient of the CNT layers. The absorption coefficient decreases with growth temperature due to the increase of the uniformity in CNTs grown at higher temperature, as was discussed in the previous section.

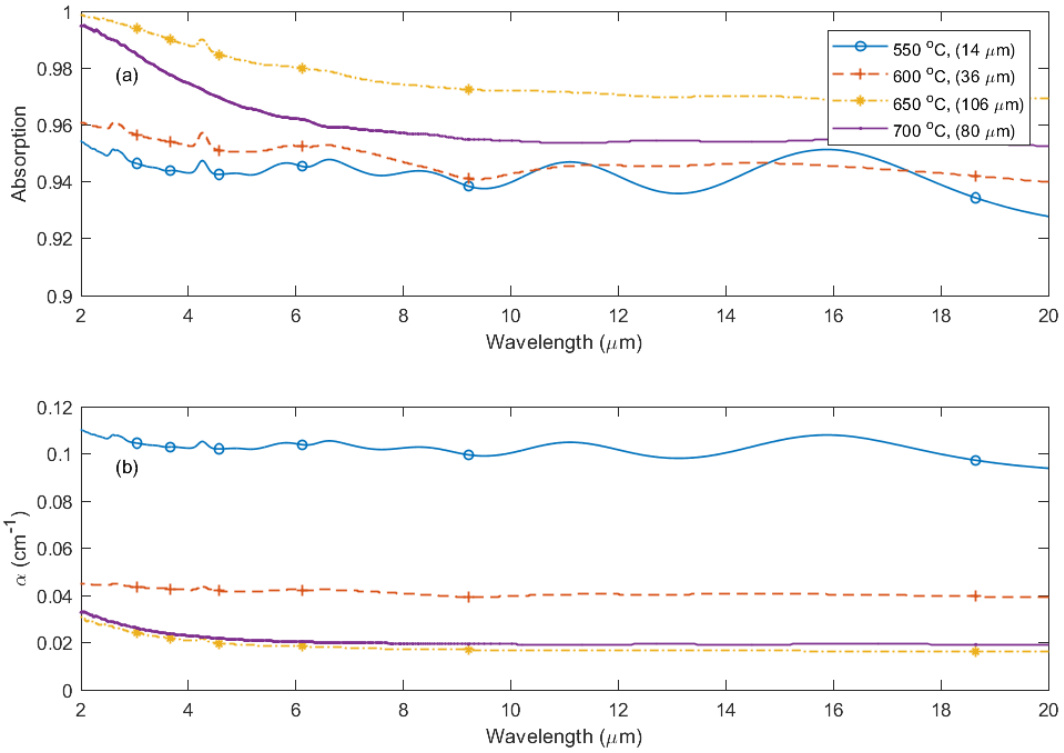

Figure 9. (a) Absorption and (b) absorption coefficient at incident angle of 15° for MWCNT forests growth at different temperatures for 10 min.

The reflectance at higher incidence angle increasingly depends on the surface quality and to a lesser degree on the height of the CNT. For instance, the SEM images in Figure 2 showed that a sample of the MWCNT grown at 700 °C has a higher roughness as compared to a sample grown at 650 °C.

Figure 10 shows the absorption coefficient at different incident angles for a 108 µm thick CNT sample grown at 650 °C. The absorption coefficient decreases with increasing incident angle [19].

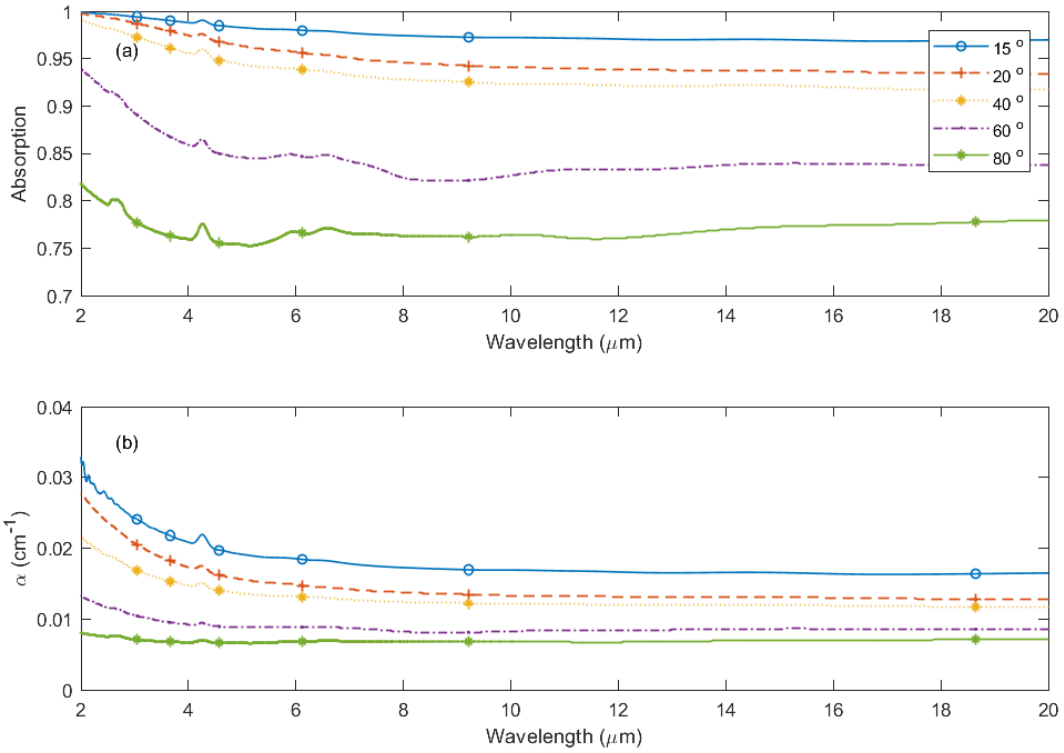

Figure 10. (a) Absorption and (b) absorption coefficient for a 100 µm thick MWCNT forests growth at 650 °C temperature at various incident angles.

3.3. Waveguide model for the optical response of MWCNT forests

Modelling the absorption coefficient of CNT forests depends on several parameters, such as the density and diameter of the nanotubes, orientation of graphite planes, and defects. A waveguide model has been introduced by Wood et al. [44] to describe the absorption properties of MWCNT by considering circular graphite waveguides. This model defines the permittivity of graphite as a weighted function of an alignment factor (X) of $\varepsilon_{\perp}$ and $\varepsilon_{\parallel}$, the radius of the waveguides (a), and a conductivity reduction factor (S_0) to describe the optical properties of the CNT.

$$\varepsilon = (n + iK)^2 = X\varepsilon_{\perp} + (1 - X)\varepsilon_{\parallel} \tag{2}$$

$$\alpha(\omega) = 2\left[\frac{P_{nm}^2}{a^2} + \frac{k^2}{P_{nm}^2 - 1}\right] \Bigg/ \left[ak\eta\sigma(\omega)\delta(\omega)\sqrt{k^2 - \frac{P_{nm}^2}{a^2}}\right] \tag{3}$$

where k is the wavenumber, P_{nm} is the mth root of the derivative of the Bessel function J_n', $\sigma(\omega) = -i\,\omega\varepsilon_0\,[\varepsilon(\omega) - 1]/S_0$ is the modified conductivity of the MWCNT, and the skin depth is $\delta(\omega) = \lambda/4\pi K$. Fitting the model with experimental data results in corresponding parameters of CNT, i. e. a, X, and, S_0 are obtained. We have used a similar guideline for fitting the model parameters. Similar density

samples are expected to have a similar waveguide diameter and S_0 value, while the permittivity changes from $\varepsilon_\perp$ to $\varepsilon_\parallel$ for thicker CNTs. The waveguide model was applied to fit the measured absorption coefficient represented in Figure 8 and 9 and provide a reasonable fit in the 3-15 μm wavelength range. The fitted absorption coefficient curves are shown in Figure 11. Whenever the fit was not unique, the parameters with the lowest radius for the waveguide was selected.

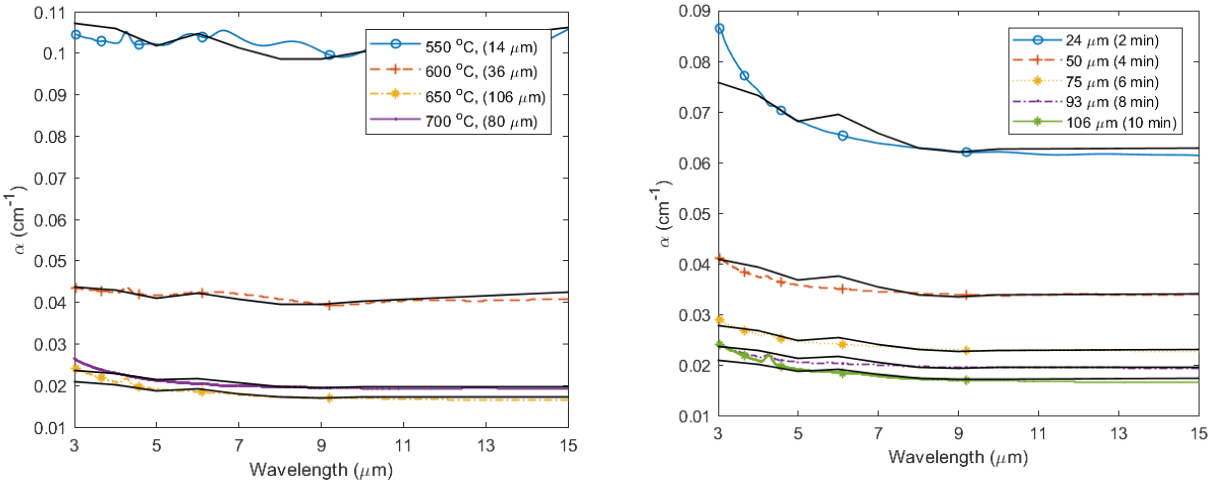

(a) (b)

Figure 11. Fitted curve (solid line) of the absorption coefficient for MWCNT layers growth at various (a) temperatures and (b) times.

Table 2 and 3 list the fit parameters. Table 2 lists the fit parameters for MWCNT layers with various thickness values grown at 650 °C, as shown in Figure 8. The waveguide diameter and the alignment factor were found to be independent of the thickness of the layer, and to be 30 μm and 1, respectively; On the other hand, the S_0 parameter decreases with increasing thickness resulting in a higher electrical conductivity. Increasing the growth temperature on the other hand increases the graphite alignment factor from 0.33 for 550 °C up to 1 for 650 °C and 700 °C, as you can see in Table 3. Therefore, CNTs grown at a temperature above 650 °C show a significantly higher contribution from the graphite basal plane. The waveguide diameter decreases significantly for the CNT layer grown at 650 °C which indicates a higher density in the layer, which is consistent with the SEM analysis.

Table 2. Fitted parameters in the waveguide model for MWCNT growth at 650 °C in various thicknesses.

Thickness (μm)	a (μm)	X	S_0
24	30	1.00	11.3
50	30	1.00	6.1
75	30	1.00	4.1
93	30	1.00	3.5
106	30	1.00	3.1

Table 3. Fitted parameters in the waveguide model for MWCNT growth in 10 min for various temperatures.

Temperature (^{o}C)	a (μm)	X	S_0
550 °C	22	0.33	7.9
600 °C	21	0.39	3.2
650 °C	30	1.00	3.1
700 °C	30	1.00	3.5

4. Conclusions

In this work, the properties of the VA-MWCNT forest as an infrared absorber were investigated as a function of synthesis parameters. VA-MWCNT layers of different thickness were grown at different temperatures and characterized using SEM, TEM, Raman, and FTIR. Quantitative Raman analysis revealed that while the thickness of the CNT has little effect on the quality, a low synthesis temperature results in more defects. The forest height increased linearly with the synthesis time and it was maximum at synthesis temperature of 650 °C. The diameter of MWCNT is found to be independent of the growth temperature and in the range of 20-30 nm. The absorption of the CNT layers was measured over the infrared spectrum, and the absorption coefficient was calculated. While the absorption was measured to be above 0.95 for all samples, the absorption coefficient varies significantly with growth temperature and time. The absorption is almost wavelength-independent for wavelengths larger than 4 μm. While the absorption is maximum and constant within ±3% for an incident angle up to 40°, the absorption decreases at higher angles of incidence due to the surface effects. Waveguide model was fitted to the measurement results. The variation of fit parameters with thickness and growth temperature showed a systematic trend. The modelling suggests that by increasing the thickness, the conductivity of the layer increases. Growth temperature however, changes the CNT quality and thus the absorption. This study may improve the understanding required for repeatable fabrication by LPCVD of highly absorbing MWCNT forest layers for promising applications in optical detectors.

Funding

This work has been supported by the research programme 4TU.HTM, 'New Horizons in Designer Materials' of the Netherlands.

References

[1] W. Niu, L.T. Su, R. Chen, H. Chen, Y. Wang, A. Palaniappan, H. Sun, A.I.Y. Tok, 3-Dimensional photonic crystal surface enhanced upconversion emission for improved near-infrared photoresponse, Nanoscale 6(2) (2014) 817-824.
[2] X. Sun, J. Zhang, X. Lu, X. Fang, H. Peng, Mechanochromic Photonic-Crystal Fibers Based on Continuous Sheets of Aligned Carbon Nanotubes, Angewandte Chemie International Edition 54(12) (2015) 3630-3634.
[3] S. Darbari, Y. Abdi, S. Mohajerzadeh, E.A. Soleimani, High electron emission from branched tree-like carbon nanotubes suitable for field emission applications, Carbon 48(9) (2010) 2493-2500.
[4] Y. Zakharko, A. Graf, S.P. Schießl, B. Hähnlein, J.r. Pezoldt, M.C. Gather, J. Zaumseil, Broadband tunable, polarization-selective and directional emission of (6, 5) carbon nanotubes coupled to plasmonic crystals, Nano letters 16(5) (2016) 3278-3284.
[5] S. Mukherjee, A. Misra, Broadband wavelength-selective reflectance and selective polarization by a tip-bent vertically aligned multi-walled carbon nanotube forest, Journal of Physics D: Applied Physics 47(23) (2014) 235501.
[6] Y. Danlée, C. Bailly, I. Huynen, Flexible polarization-dependent absorbers based on patterned carbon nanotubes films, Microwave and Optical Technology Letters 59(5) (2017) 1164-1167.
[7] A. Lin, C.-C. Yang, P. Parashar, C.-Y. Lin, D.R. Jian, W.-M. Huang, Y.-W. Huang, S.M. Fu, Y.K. Zhong, T.Y. Tseng, An ultra-compact blackbody using electrophoretic deposited carbon nanotube films, RSC Advances 8(7) (2018) 3453-3461.
[8] N. Selvakumar, S. Krupanidhi, H.C. Barshilia, Carbon Nanotube-Based Tandem Absorber with Tunable Spectral Selectivity: Transition from Near-Perfect Blackbody Absorber to Solar Selective Absorber, Advanced Materials 26(16) (2014) 2552-2557.
[9] Z.M. Zhang, H. Ye, Measurements of radiative properties of engineered micro-/nanostructures, Annual Review of Heat Transfer 16(1) (2013).
[10] J. Wei, Y. Jia, Q. Shu, Z. Gu, K. Wang, D. Zhuang, G. Zhang, Z. Wang, J. Luo, A. Cao, Double-walled carbon nanotube solar cells, Nano letters 7(8) (2007) 2317-2321.
[11] R. Fainchtein, D.M. Brown, K.M. Siegrist, A.H. Monica, E. Hwang, S.D. Milner, C.C. Davis, Time-dependent near-blackbody thermal emission from pulsed laser irradiated vertically aligned carbon nanotube arrays, Physical Review B 85(12) (2012) 125432.
[12] Y. Shimizu, J. Ishii, Blackbody thermal radiator with vertically aligned carbon nanotube coating, Japanese Journal of Applied Physics 53(6) (2014) 068004.
[13] T. Akutsu, Y. Saito, Y. Sakakibara, Y. Sato, Y. Niwa, N. Kimura, T. Suzuki, K. Yamamoto, C. Tokoku, S. Koike, Vacuum and cryogenic compatible black surface for large optical baffles in advanced gravitational-wave telescopes, Optical Materials Express 6(5) (2016) 1613-1626.
[14] Y.D. Lim, L. Hu, A.V. Avramchuck, D. Grapov, B.K. Tay, S. Aditya, J. Miao, V. Labunov, Temperature-dependent selective growth of carbon nanotubes in Si/SiO2 structures for field emitter array applications, Materials Research Bulletin 95 (2017) 129-137.
[15] Y. Deng, Q. Sun, J. Yu, Y. Lin, J. Wang, Broadband high-absorbance coating for terahertz radiometry, Optics express 21(5) (2013) 5737-5742.
[16] J.K. Streit, S.M. Bachilo, S. Ghosh, C.-W. Lin, R.B. Weisman, Directly measured optical absorption cross sections for structure-selected single-walled carbon nanotubes, Nano letters 14(3) (2014) 1530-1536.

[17] S. Zhang, L. Kang, X. Wang, L. Tong, L. Yang, Z. Wang, K. Qi, S. Deng, Q. Li, X. Bai, Arrays of horizontal carbon nanotubes of controlled chirality grown using designed catalysts, Nature 543(7644) (2017) 234.
[18] J. Lehman, A. Sanders, L. Hanssen, B. Wilthan, J. Zeng, C. Jensen, Very black infrared detector from vertically aligned carbon nanotubes and electric-field poling of lithium tantalate, Nano letters 10(9) (2010) 3261-3266.
[19] Z.-P. Yang, L. Ci, J.A. Bur, S.-Y. Lin, P.M. Ajayan, Experimental observation of an extremely dark material made by a low-density nanotube array, Nano letters 8(2) (2008) 446-451.
[20] A.A. Puretzky, D.B. Geohegan, S. Jesse, I.N. Ivanov, G. Eres, In situ measurements and modeling of carbon nanotube array growth kinetics during chemical vapor deposition, Applied Physics A 81(2) (2005) 223-240.
[21] H. Ye, X.J. Wang, W. Lin, C.P. Wong, Z.M. Zhang, W. Z., C. Z., D. X., L.J. M., S. J., N. M., K. K., R.J. R., T.D. B., H.A. F., R.A. G., Infrared absorption coefficients of vertically aligned carbon nanotube films, Applied Physics Letters 101(14) (2012) 141909.
[22] K.-C. Hsieh, T.-Y. Tsai, D. Wan, H.-L. Chen, N.-H. Tai, Iridescence of Patterned Carbon Nanotube Forests on Flexible Substrates: From Darkest Materials to Colorful Films, ACS Nano 4(3) (2010) 1327-1336.
[23] M.R.M. Asyraf, M.M. Rana, T. Saleh, H.D.E. Fan, A.T. Koch, A. Nojeh, K. Takahata, A.B. Suriani, Study on micro-patterning process of vertically aligned carbon nanotubes (VACNTs), Fullerenes, Nanotubes and Carbon Nanostructures 24(2) (2016) 88-99.
[24] T. Saleh, M.V. Moghaddam, M.S. Mohamed Ali, M. Dahmardeh, C.A. Foell, A. Nojeh, K. Takahata, Transforming carbon nanotube forest from darkest absorber to reflective mirror, Applied Physics Letters 101(6) (2012) 061913.
[25] M. Rana, M.R.M. Asyraf, T. Saleh, A.G.A. Muthalif, Investigation of anisotropic reflectance from densified arrays of vertically aligned carbon nanotube forests (VACNTs), Chemical Physics Letters 658 (2016) 343-346.
[26] M. Wąsik, J. Judek, M. Zdrojek, Polarization-dependent optical reflection from vertically aligned multiwalled carbon nanotube arrays, Carbon 64 (2013) 550-552.
[27] G. Rahman, Z. Najaf, A. Mehmood, S. Bilal, A.u.H.A. Shah, S.A. Mian, G. Ali, An Overview of the Recent Progress in the Synthesis and Applications of Carbon Nanotubes, C — Journal of Carbon Research 5(1) (2019) 3.
[28] A. Javid, K. Avshish, H. Samina, K. Monika, Harsh, H. Mushahid, Characterization and Field Emission Studies of Uniformly Distributed Multi-Walled Carbon Nanotubes (MWCNTs) Film Grown by Low-pressure Chemical Vapour Deposition (LPCVD), Current Nanoscience 7(3) (2011) 333-336.
[29] S. Santangelo, M. Lanza, E. Piperopoulos, S. Galvagno, C. Milone, Optimization of CVD growth of CNT-based hybrids using the Taguchi method, Materials Research Bulletin 47(3) (2012) 595-601.
[30] S. Vollebregt, F.D. Tichelaar, H. Schellevis, C.I.M. Beenakker, R. Ishihara, Carbon nanotube vertical interconnects fabricated at temperatures as low as 350°C, Carbon 71 (2014) 249-256.
[31] J.H. Lehman, M. Terrones, E. Mansfield, K.E. Hurst, V. Meunier, Evaluating the characteristics of multiwall carbon nanotubes, Carbon 49(8) (2011) 2581-2602.
[32] S.K. Pal, S. Talapatra, S. Kar, L. Ci, R. Vajtai, T. Borca-Tasciuc, L.S. Schadler, P.M. Ajayan, Time and temperature dependence of multi-walled carbon nanotube growth on Inconel 600, Nanotechnology 19(4) (2008) 045610.

[33] S.M. Ubnoske, E.J. Radauscher, E.R. Meshot, B.R. Stoner, C.B. Parker, J.T. Glass, Integrating carbon nanotube forests into polysilicon MEMS: Growth kinetics, mechanisms, and adhesion, Carbon 113 (2017) 192-204.
[34] E.F. Antunes, A.O. Lobo, E.J. Corat, V.J. Trava-Airoldi, A.A. Martin, C. Veríssimo, Comparative study of first- and second-order Raman spectra of MWCNT at visible and infrared laser excitation, Carbon 44(11) (2006) 2202-2211.
[35] S. Vollebregt, R. Ishihara, F.D. Tichelaar, Y. Hou, C.I.M. Beenakker, Influence of the growth temperature on the first and second-order Raman band ratios and widths of carbon nanotubes and fibers, Carbon 50(10) (2012) 3542-3554.
[36] A.C. Ferrari, J. Robertson, Raman spectroscopy of amorphous, nanostructured, diamond–like carbon, and nanodiamond, Philosophical Transactions of the Royal Society of London. Series A: Mathematical, Physical and Engineering Sciences 362(1824) (2004) 2477-2512.
[37] R.A. DiLeo, B.J. Landi, R.P. Raffaelle, Purity assessment of multiwalled carbon nanotubes by Raman spectroscopy, Journal of Applied Physics 101(6) (2007) 064307.
[38] N.G. Shang, Y.Y. Tan, V. Stolojan, P. Papakonstantinou, S.R.P. Silva, High-rate low-temperature growth of vertically aligned carbon nanotubes, Nanotechnology 22(9) (2011) 099801.
[39] F.H. Kaatz, M.P. Siegal, D.L. Overmyer, P.P. Provencio, D.R. Tallant, Thermodynamic model for growth mechanisms of multiwall carbon nanotubes, Applied Physics Letters 89(24) (2006) 241915.
[40] Z. Yang, Q. Zhang, G. Luo, J.-Q. Huang, M.-Q. Zhao, F. Wei, Coupled process of plastics pyrolysis and chemical vapor deposition for controllable synthesis of vertically aligned carbon nanotube arrays, Applied Physics A 100(2) (2010) 533-540.
[41] Q.N. Pham, L.S. Larkin, C.C. Lisboa, C.B. Saltonstall, L. Qiu, J.D. Schuler, T.J. Rupert, P.M. Norris, Effect of growth temperature on the synthesis of carbon nanotube arrays and amorphous carbon for thermal applications, physica status solidi (a) 214(7) (2017) 1600852.
[42] M.M. Rahman, H. Younes, G. Ni, T. Zhang, A. Al Ghaferi, Synthesis and optical characterization of carbon nanotube arrays, Materials Research Bulletin 77 (2016) 243-252.
[43] K. Mizuno, J. Ishii, H. Kishida, Y. Hayamizu, S. Yasuda, D.N. Futaba, M. Yumura, K. Hata, A black body absorber from vertically aligned single-walled carbon nanotubes, Proceedings of the National Academy of Sciences 106(15) (2009) 6044-6047.
[44] J.S.D. B. D. Wood, V. A. Thurgood, N. A. Tomlin, J. H. Lehman, and T.-C. Shen, Optical reflection and absorption of carbon nanotube forest films on substrates, Journal of Applied Physics 118(1) (2015) 013106.